Modifications of Graphitic C_3N_4 with Multi-metal Oxides for Enhanced Visible-light Active Photocatalysis

Dilshad Masih, Yuanyu Ma and Sohrab Rohani*

Department of Chemical & Biochemical Engineering, University of Western Ontario, London, ON, Canada, *E-mail: srohani@uwo.ca

ABSTRACT

Graphitic C_3N_4 (g-C_3N_4) was modified by doping with zinc and construction of heterostructures with silver and copper-vanadium oxides. XRD patterns revealed that graphitic structure of C_3N_4 was maintained after modifications. Besides new diffraction peaks appeared for the copper-vanadium oxide phase. However, upon modifications with zinc and silver no appreciable new peaks were observed in the XRD patterns. Vibrational spectroscopy investigations showed signature IR peaks for g-C_3N_4 and furher supported the findings in the XRD patterns. Red-shift upon modifications of g-C_3N_4 demonstrated better absorbance of visible-light. Thermogravimetry analysis showed weight loss for copper-vanadate phase transformation around 520 K, and decomposition temperature of g-C_3N_4 around 950 K that decreased with loading of metal/metal oxides. Photocatalysis effeciency of catalysts was evaluated by aqueous phase mineralization of Rhodamine B under visible-light irradation.

Keywords: g-C_3N_4, multi-metal oxides, heterostructure, photocatalysis

1 INTRODUCTION

Polymeric material g-C_3N_4 is getting increased attention as a metal free catalyst [1-5]. Bulk g-C_3N_4 is a *p*-type semiconductor with band gap of 2.7 eV [1, 2]. For photocatalytic water splitting, valance and conduction band gap positions of g-C_3N_4 sandwich both oxygen and hydrogen evolution potentials, making g-C_3N_4 an important material for further investigations [3-5]. In recent years, various modifications of g-C_3N_4 toward development of a sustainable catalyst are hot topic of research on harvesting solar energy for environment and energy sectors [2-7]. However, separation of photo-excited electron and hole pairs is an intrinsic problem with bulk g-C_3N_4. Control of g-C_3N_4 morphology helps in increasing the number of active sites upon formation of a mesoporous structure, and separation of electrons and holes in its graphene analogous nanosheets in the UV range. Doping and fabrication of heterojunctions are the main approaches for enhanced separation followed migration of electron and hole pairs onto the surface, and consequently their use in photocatalytic reactions. Moreover, band gap engineering of g-C_3N_4 with suitable plasmonic and semiconductor materials helps in extended optical absorption of visible-light and efficient photocatalysis.

Multi-metal oxides in d^0 and d^{10} electronic configurations are interesting narrow band gap semiconductor for harvesting solar energy [8, 9]. However, poor separation of electron and hole pairs along with their instability under experimental conditions pose serious problems. Formation of multi-metal oxides of group V (d^0) with copper/silver (d^{10}) metals, and fabrication of their heterojunctions with g-C_3N_4 may help in development of stable and efficient visible-light active photocatalyst systems. Copper based ternary oxides and various metal-vandates have been explored for the ehancement of photocatalytic effeciency of g-C_3N_4 [10-13]. Doping with metal/non-metal and surface decoration as a co-catalyst are reported separately for the modifications of g-C_3N_4 [14-17]. We tried new facile route for silver loading onto a zinc doped g-C_3N_4. New hybrid photocatalyst systems of g-C_3N_4 with copper-vanadium oxide, and of zinc doped g-C_3N_4 with silver are investigated in this study.

2 EXPERIMENTAL

Reagent grade melamine (99%; Aldrich), $Cu(NO_3)_2.xH_2O$ (98%; Alfa Aesar), NH_4VO_3 (99%; Aldrich), $ZnSO_4.7H_2O$ (99%; Caledon) and $AgNO_3$ (99%; Caledon) were used in synthesis of catalyst materials. Absolute ethanol (Aldrich) and deionized water were used as solvents. Rhodamine B (99%; Acros) was used as a model organic dye for catalytic photodegradation testing.

2.1 Synthesis of Catalysts

Pure g-C_3N_4 was synthesized by calcination of melamine in alumina crucible with a cover. Solid-state reaction was carried out at 823 K for 4 h. For zinc doped g-C_3N_4, clear solution of zinc salt in ethanol was mixed with melamine suspension, and refluxed at 333 K for 4 h. Then ethanol was allowed to evaporate and obtained powder was calcined at 823 K for 4 h. Subsequently, g-C_3N_4 and zinc doped g-C_3N_4 were modified with silver, and copper-vanadium oxide in aqueous phase. Copper-vanadium oxide heterostructures with g-C_3N_4 were fabricated by in-situ growth, and also by deposition of ex-situ formed species.

Metal precursors were dissolved in water and sequentially mixed with g-C_3N_4 suspension followed by reflux at 353 K for 4–6 h. Then water was allowed to evaporate at 373 K, and dried materials were grinded to fine powder. Thus obtained materials were used for characterization by various techniques, and for photocatalytic testing.

2.2 Characterization of Catalysts

Powder XRD patterns were recorded using a Rigaku diffractometer, model MiniFlex. Vibratioal spectra were measured with ATR mode on Bruker spectrometer, model Vector 22. Cary spectrophotometer, model 100 Bio was used for optical investigations on the materials, and for quantification of dye contents during photocatalytic testing. Thermogravimetric-diffrential thermal analysis (TG-DTA) in alumina crucible with a cover was performed on Mettler Toledo instrument, model TGA/SDTA851.

2.3 Photocatalysis Test

100 mg of catalyst powder was suspended in 100 ml aqueous solution of Rhodamine B, and stirred in dark for 30 min. Then the mixture was exposed to light from Newport solar simulator, model 67005 operating at 150 W and adjusted to 1 sun illumination. Small aliquots were drawn from the reaction mixtrue at regular intervals to access the photodegradation of Rhodamine B by UV-Vis spectrophotometer.

3 RESULTS & DISCUSSION

3.1 Physicochemical Properties

Powder XRD patterns with main peak around 27.6° demonstrated well formed graphitic structure of pure and zinc doped C_3N_4. For the heterostructure with copper-vanadium oxide (CuV_2O_X), g-C_3N_4 structure was maintained while new diffraction peaks appeared for the mixed-metal oxide as shown in Figure 1.

Characterisitic diffraction peak from CuV_2O_X was observed at 11.5°. Along with CuV_2O_X, diffraction peaks from NH_4NO_3 were also observed even though product was dried at 373 K overnight. Intensity of main diffraction peak of g-C_3N_4 (27.6°) was decreasing with increasing loading of CuV_2O_X from 0–20 wt.%. Structure regularity of g-C_3N_4 also decreased after doping with zinc, and loading with silver species. For up to 5 wt.% loading with silver, no appreciable diffraction peak was observed for metallic silver and/or its oxide species.

Figure 2 depicts infrared (IR) spectra of g-C_3N_4, CuV_2O_X and for their heterostructures. Signature IR absorbance in the wavenumber range of 1700–900 cm^{-1}, and a sharp feature around 800 cm^{-1} confirmed the graphitic structure of C_3N_4, as seen in the XRD patterns.

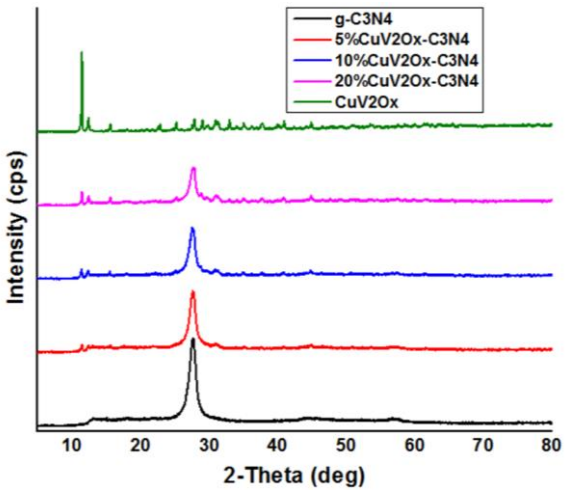

Figure 1: XRD patterns of g-C_3N_4, CuV_2O_X, and their heterostructures.

Two new features corresspoding to CuV_2O_X species started to develop at 1000 cm^{-1} and 965 cm^{-1}. Absorbance of IR for these new features increased with loading of CuV_2O_X in g-C_3N_4. Similarly, graphitic structure of C_3N_4 was maintained before and after doping with zinc, and loading with silver. Essentially, no new IR band was observed after doping with zinc and loading with silver.

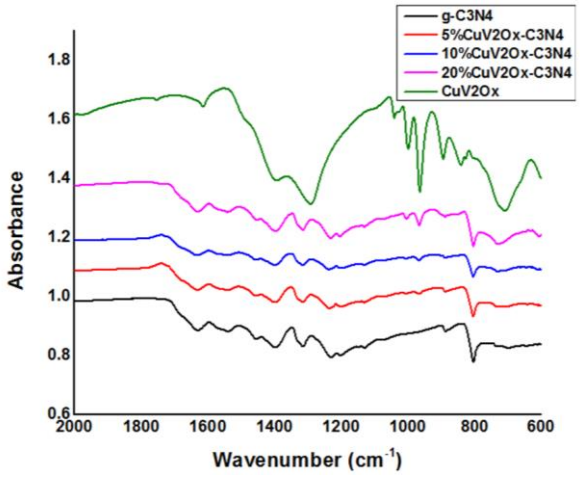

Figure 2: Infrared spectra of g-C_3N_4, CuV_2O_X, and their heterostructures.

Diffuse reflectance UV-Vis (DR-UV-Vis) spectra of powder catalysts are illustrated in Figure 3. These spectra gave important feedback towards their application in harvesting solar energy. Absorption edge for pure g-C_3N_4 was observed in the visible region above 400 nm, corresponding to its yellow color and band gap of 2.7 eV. Next for CuV_2O_X, absorption edge was located around 510 nm demonstrating its narrow band gap compared to that of g-C_3N_4. A new peak feature between 440–540 nm was observed in the heterostructures of g-C_3N_4 with CuV_2O_X.

As shown in Figure 3, visible-light absorbance for the hybrid structure increased in between 440–540 nm with increasing wt.% of CuV_2O_X. A red-shift in the absorption edge of g-C_3N_4 is demonstrated upon formation of its heterostructures with CuV_2O_X. Consequently, making g-C_3N_4 and CuV_2O_X hybrid structures is more suitable for harvesting visible-light. Similarly, optical studies on zinc doped g-C_3N_4 and its modifications with silver demonstrated better prospects of hybrid structures in harvesting solar energy.

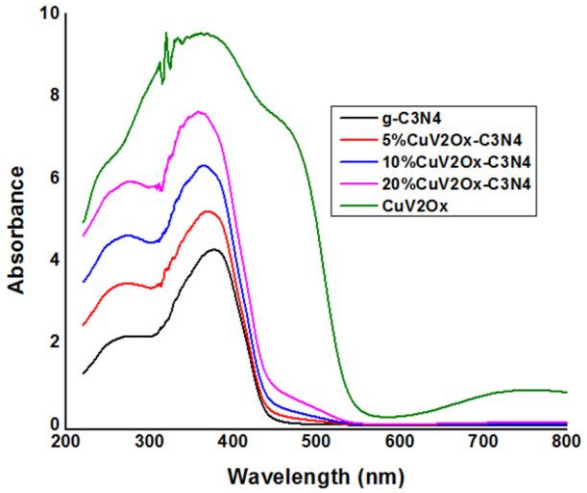

Figure 3: DR-UV-Vis spectra of g-C_3N_4, CuV_2O_X, and their heterostructures.

TG-DTA studies on pure and zinc doped g-C_3N_4 before and after formation of heterostructures with multi-metal oxides explained the changes in structure and phase of the materials at different temperatures. Thermogravimetry curves for g-C_3N_4, CuV_2O_X, and their hybrid structures are shown in Figure 4. In the TG curve for pure g-C_3N_4, a sharp decomposition temperature (around 950 K) showed almost complete, 98% loss of its weight.

DTA profile for g-C_3N_4 showed an endothermic behavior of the reaction of its decomposition, around 950 K. For pure CuV_2O_X, weight loss of about 10% in between 350–500 K occurred due to the removal of water and NH_4NO_3. A sharp TG curve around 520 K with a further 25% weight loss demonstrated the formation of CuV_2O_6, and XRD analysis confirmed this phase change. DTA profile for removal of water and NH_4NO_3 showed endothermic reaction, while for the formation of CuV_2O_6 phase it exhibited an exothermic behavior.

As depicted in the TG curves for g-C_3N_4 and CuV_2O_X heterostructures, the onset temperature for the formation of CuV_2O_6 phase was about 20 K lower than that for its transformation in pure phase. Similarly, temperature for decomposition of C_3N_4 in the hybrid systems was about 60 K (20%CuV_2O_x-C_3N_4) lower than that of the pure g-C_3N_4. A trend in the lowering down of the decomposition temperature of C_3N_4 was observed against the CuV_2O_X loading in the hybrid systems. For the zinc doped and silver loaded g-C_3N_4 samples, the TG curves also showed a decrease in the decomposition temperature of C_3N_4. TG-DTA and XRD studies provided important information on required conditions for thermal treatments in constructing semiconductor-semiconductor heterojunctions.

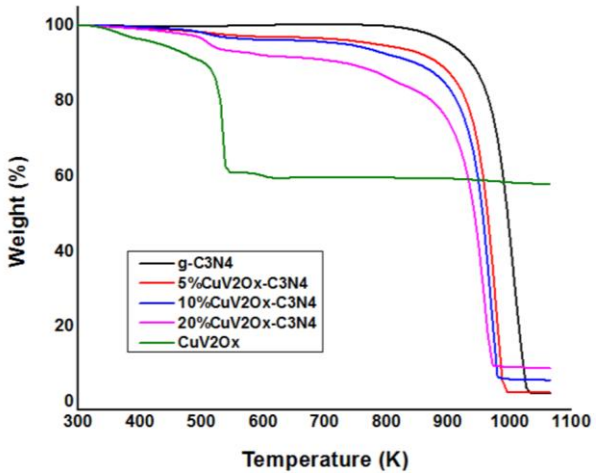

Figure 4: Thermogravimetry curves for g-C_3N_4, CuV_2O_X, and their heterostructures.

3.2 Visible-light Active Photodegradation

Photodegradation of Rhodamine B, a cationic dye was performed over the synthesized materials under 1 sun illumination. Optical properties (Figure 3) demonstrated that absorption for these materials was essentially in the visible region, so their catalytic efficiencies were examined under illumination from a solar simulator.

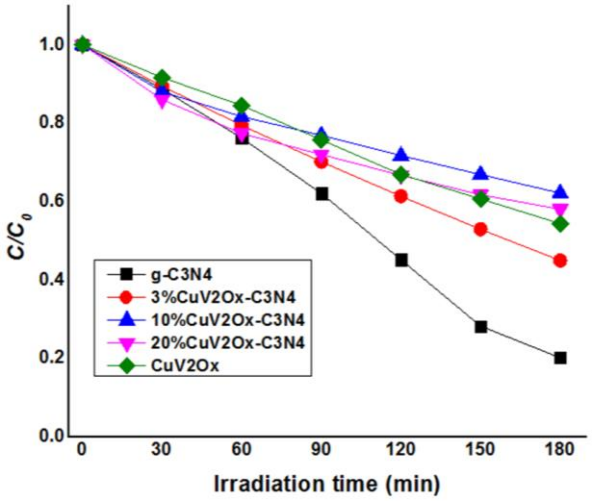

Figure 5: Visible-light active photodegradation of Rhodamine B over g-C_3N_4, CuV_2O_X, and their heterostructures.

For a 30 min equilibration process of Rhodamine B sorption/degradation in dark, no appreciable decrease in the dye contents was observed over pure, zinc doped, and multi-metal oxide modified g-C_3N_4 systems. It is important to note that catalyst powders of CuV_2O_X, and its hybrid structures with g-C_3N_4 formed a thin layer of particles on the surface of the aqueous Rhodamine B reaction mixture, demonstrating their hydrophobic nature.

Figure 5 depicts visible-light active photodegradation over g-C_3N_4, CuV_2O_X, and their hybrid structures. Initial rate of reaction for irradiation time around 30 min is similar for all the catalysts. Beyond 60 min irradiation, mineralization of Rhodamine B proceeded relatively faster on g-C_3N_4 than that on the CuV_2O_X based cataysts. No synergy was found for Rhodamine B photodegradation over heterostructures of g-C_3N_4 with CuV_2O_X. The transformed phase of CuV_2O_X catalyst, CuV_2O_6 (as illustrated by TG-DTA and XRD studies), might lead to efficient degradation of environmental pollutants and water splitting.

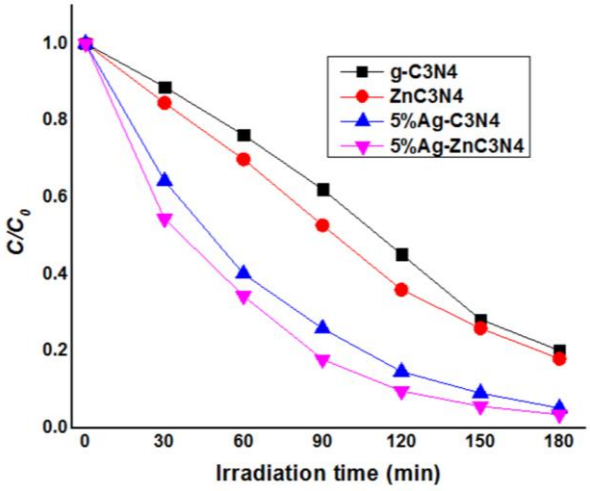

Figure 6: Visible-light active photodegradation of Rhodamine B over pure and zinc doped g-C_3N_4, before and after silver loading.

Results for visible-light active photodegradation of Rhodamine B over pure, zinc doped g-C_3N_4 with and without silver loadings are shown in Figure 6. Zinc doping of g-C_3N_4 enhanced the rate of photodegradation of the organic pollutant. Next, mineralization of Rhodamine B over silver loaded materials proceeded relatively faster than the samples without silver. Importantly, silver species acted as a co-catalyst and helped with the migration of photo-excited electrons on to the surface of g-C_3N_4, avoiding their recombinations. Consequently, rate of visible-light active photodegradation of Rhodamine B increased for the semiconductors with co-catalysts. Overall, zinc doped g-C_3N_4 and loaded with 5 wt.% silver demonstrated the highest effeciency, almost 98% photodegradation of Rhodamine B in 180 min. Photo-corrosion of silver loaded g-C_3N_4 samples was noticed during catalytic testing. Hence, further modifications are indispensable for fabrication of greener photocatalysts with repeated usage.

4 CONCLUSIONS

Heterostructures of g-C_3N_4 with various compositions of copper-vandium oxide were fabricated successfully under facile conditions. Detailed characterizations, especially TG-DTA and XRD demonstrated suitable conditions for appropriate thermal treatments of hybrid structures in making the materials more effective for harvesting solar energy. Layred structure of g-C_3N_4 was retained after modifications, and absorption of visible-light by hybrid strcutures was extended to wider range of wavelength. Zinc doped g-C_3N_4 with silver co-catalyst exhibited the most efficient photodegradation of Rhodamine B under visible-light illumination.

REFERENCES

[1] A. Thomas, A. Fischer, F. Goettmann, M. Antonietti, J. O. Muller, R. Schlogl and J. M. Carlsson, J. Mater. Chem., 18, 4893 – 4908, 2008.

[2] Y. Wang, X. Wang and M. Antonietti, Angew. Chem. Int. Ed., 51, 68–89, 2012.

[3] J. Zhu, P. Xiao, H. Li and S. A. C. Carabineiro, ACS Appl. Mater. Interfce., 6, 16449–16465, 2014.

[4] G. Dong, Y. Zhang, Q. Pan and J. Qiu, J. Photochem. Photobiol. C: Photochem. Rev., 20, 33–50, 2014.

[5] S. Cao, J. Low, J. Yu and M. Jaroniec, Adv. Mater., 27, 2150–2176, 2015.

[6] X. Wang, S. Blechert and M. Antonietti, ACS Catalysis, 2, 1596–1606, 2012.

[7] Z. Zhao, Y. Sun and F. Dong, Nanoscale, 7, 15–37, 2015.

[8] Y. Zheng, L. Lin, B. Wang and X. Wang, Angew. Chem. Int. Ed., 54, 12868–12884, 2015.

[9] U. A. Joshi, A. Palasyuk, D. Arney and P. A. Maggard, J. Phys. Chem. Lett., 1, 2719–2726, 2010.

[10] M. Harb, D. Masih and K. Takanabe, Phys. Chem. Chem. Phys., 16, 18198–18204, 2014.

[11] S. Z. Wu, K. Li and W. D. Zhang, Appl. Surf. Sci., 324, 324–331, 2015.

[12] H. Shi, C. Zhang and C. Zhou, RSC Adv., 5, 50146–50154, 2015.

[13] Y. Yao, F. Lu, Y. Zhu, F. Wei, X. Liu, C. Lian and S. Wang, J. Hazard. Mater., 297, 224–233, 2015.

[14] R. Cheng, X. Fan, M. Wang, M. Li, J. Tian and L. Zhang, RSC Adv., 6, 18990–18995, 2016.

[15] B. Yue, Q. Li, H. Iwai, T. Kako and J. Ye, Sci. Technol. Adv. Mater., 12, 034401, 2011.

[16] J. Xu, K. Z. Long, Y. Wang, B. Xue and Y. X. Li, Appl. Catal. A: Gen., 496, 1–8, 2015.

[17] X. Lu, J. Shen, Z. Wu, J. Wang and J. Xie, J. Mater. Res., 29, 2170–2178, 2014.